Nat. Hazards Earth Syst. Sci. Discuss., 1, 5779–5804, 2013
www.nat-hazards-earth-syst-sci-discuss.net/1/5779/2013/
doi:10.5194/nhessd-1-5779-2013

Natural Hazards and Earth System Sciences
Open Access
Discussions

Numerical modeling of rogue waves in coastal waters

A. Sergeeva[1,2], **A. Slunyaev**[1,2], **E. Pelinovsky**[1,2,3], **T. Talipova**[1,2], **and D.-J. Doong**[4]

[1]Institute of Applied Physics, Nizhny Novgorod, Russia
[2]Nizhny Novgorod State Technical University, Nizhny Novgorod, Russia
[3]Johannes Kepler University, Linz, Austria
[4]National Taiwan Ocean University, Keelung, Taiwan

Received: 6 September 2013 – Accepted: 2 October 2013 – Published: 22 October 2013

Correspondence to: A. Sergeeva (a.sergeeva@hydro.appl.sci-nnov.ru)

Published by Copernicus Publications on behalf of the European Geosciences Union.

Abstract

The spatio-temporal evolution of rogue waves measured in Taiwanese coastal waters is reconstructed by means of numerical simulations; their lifetimes are estimated at up to 100 s. The reconstructed time series were measured at different locations (with dimensionless depths within the range $kh = 1.3...4.0$, where k is the wavenumber and h is the depth), but all are surprisingly weakly nonlinear waves. The variable-coefficient approximate evolution equations, which take into account the shoaling effect, allow us to analyze the abnormal wave evolution in essentially non-uniform conditions of real coastal bathymetry. The reconstruction reveals an interesting peculiarity of the coastal rogue events: though the mean wave amplitudes get amplified as waves travel onshore, other rogue waves are likely to occur at deeper locations, but not closer to the coast (the shallowest simulated point is characterized by $kh \approx 0.7$).

1 Introduction

This paper is dedicated to the analysis of rogue wave occurrences registered by buoys near the coast of Taiwan, and to reproduction of the events with the help of hydrodynamic equations. The long-term measurements of the surface displacement by several buoys moored at different locations around Taiwan resulted in a collection of time series characterizing the wave conditions in Taiwanese coastal waters (Lee et al., 2011). This dataset was analyzed from the general point of view in Doong et al. (2012); in particular, rogue waves, which exceed the surrounding waves twice or more, have been sorted out and analyzed. The rogue (or freak) waves are the threat, which has been recognized rather recently, and nowadays attracts much attention, see for reviews Kharif and Pelinovsky (2003), Dysthe et al. (2008), Kharif et al. (2009) and Slunyaev et al. (2011).

Measurements of the surface elevation at a certain point provide only limited information about waves. The time series, which contain rogue waves, by their own

NHESSD

1, 5779–5804, 2013

give no knowledge about the dynamics of the dangerous waves. In fact, much more information could be collected if quite reasonable assumptions are got involved. The first conjecture which may be made is that waves propagate unidirectionally, what implies that the angle spectrum is negligibly narrow (it is sufficient to fulfill this requirement within some reasonable short period of time, for example, for the duration of typical time series, 10–20 min, or even shorter), simultaneously no opposite waves (for example, reflected waves) are admitted. Under this assumption the surface wave dynamics takes place in one horizontal direction, and the boundary value problem becomes in principle treatable. Numerical modeling, which reconstructs the wave evolution on the basis of instrumental records, was performed in Trulsen (2001), Divinsky et al. (2004), Slunyaev et al. (2005, 2013b) and Slunyaev (2006) by means of approximate evolution equations for modulated waves. As a result of the numerical simulations, the full wave information in the vicinity of the point of measurement is obtained, the rogue wave evolution gets recovered. It is crucial that in Slunyaev et al. (2013b) the application of the weakly nonlinear theory for wave modulations was shown able to produce reliable results even in cases of very steep modulated waves. The interval of credible reconstruction of the wave dynamics was estimated at about 10 min.

An important feature of the measured time series, which are in the focus of the present paper, is variable bathymetry: the sea should be considered as a finite-depth basin, and the depth variation is essential. The complicated picture of nonlinear wave effects, when they travel from deep to shallow water was revealed by Sergeeva et al. (2011), Zeng and Trulsen (2012) and Trulsen et al. (2012). Though nonlinear wave interactions in constant-depth conditions had been believed to trigger more rogue waves than could be predicted according to the linear quasi-Gaussian statistics, the publications proved that variable depth conditions were able to further increase the rogue wave probability.

In this paper we consider four time series measured in the coastal waters of Taiwan, which contain rogue waves. In order to understand the nonlinear dynamics

NHESSD
1, 5779–5804, 2013

of extreme waves coming from the open sea to the coast and to assess the rogue wave danger throughout the coast, we reconstruct the wave evolution of the in-situ rogue waves employing the nonlinear theory for modulated waves. In Sect. 2 the conditions of measurements and the field data are briefly described. The employed evolution equations and the approach, how the in-situ time series serve the initialization of the numerical codes, are introduced in Sect. 3. Section 4 provides the results of the simulations, and the outcomes are summarized in Sect. 5.

2 Field data

The long-term instrumental measurements of waves in the coastal ocean of Taiwan have been conducted since 1997 by Taiwanese Central Weather Bureau (CWB) and Water Resources Agency (WRA) (Doong et al., 2007). Currently there are 15 data buoys in operation at Taiwanese Waters. The records used in this study are retrieved from those buoys moored at several locations, which differ in the distance offshore, local depth, currents, typical wave spectra, etc. The sampling rate of the buoys on their movements is 2 Hz. The 512 s series of surface elevations are extracted by wavelet transform (Lee et al., 2011). An extensive analysis of the available dataset has been performed in Chang (2012). It exhibits a rich variety of rogue wave appearances. In average, there are about 100 rogue waves measured at those buoys. The occurrence probability is from $1.7 \sim 2.1 \times 10^{-4}$, means one rogue wave occurs in every 5000 waves. The conventional criterion for rogue waves was used,

$$\mathrm{AI} \equiv \frac{H}{H_s} > 2, \tag{1}$$

where H is the wave height and H_s is the significant wave height. This criterion will be used throughout the paper, where the quantity AI will be referred to as abnormality index. If there is a typhoon (tropical cyclone) close to the station, the occurrence

NHESSD
1, 5779–5804, 2013

probability of measured rogue waves increase 2–7 times compared to ordinary days. It was also found that the percentage of rogue waves with symmetric shapes is large.

Four samples of the time series from the dataset were picked out for the present study, see Figs. 1 and 2. The rogue waves represent three kinds of wave geometry: so-called "holes in the sea" due to deep troughs in Fig. 2a and c (Hsinchu and Eluanbi stations), a sign-variable wave in Fig. 2b (Hualien station) and a high-crested wave in Fig. 2d (Longdong station). The distances to shore, $-x_0$, for the measuring stations are given in Table 1 together with the local depth, h, and other related parameters. Periods of the rogue waves are $T_{fr} = 6–10$ s, where the subscript fr will denote the rogue (or freak) wave characteristics. The peak periods, T_p, are obtained from the frequency spectra, hence every record contains from 53 to 78 periods T_p. Three of the situations correspond to the intermediate depth with dimensionless depths, $k_p h$, within the range 1.3 ... 2.3, and the fourth buoy (Longdong) is moored at the deep water location with $k_p h = 4$. Here k_p, is determined from the peak angular frequency, ω_p, through the dispersion relation for gravity waves over finite depth,

$$\omega^2 = gk \tanh(kh). \quad (2)$$

The significant wave heights and rogue wave heights and crest heights, H_{cr}, are given in Table 1. The characteristic wave steepness estimated through the standard deviation of the surface elevation, η_{rms}, as $\varepsilon = k_p \eta_{rms}$, varies from 0.02 to 0.04, which corresponds to rather weak nonlinearity. The steepness of the rogue wave may be estimated with the help of the local wave length, λ_{fr} (again, related to the local zero-crossing wave period according to the dispersion relation Eq. 2), and the crest height; then the rogue wave steepness is estimated as $k_{fr} H_{cr} = 0.08 \ldots 0.15$. All this certifies the weakly nonlinear nature of the measured abnormal waves.

For the purpose of numerical simulation of wave propagation onshore and offshore, the real bathymetry is used. For each the buoy the coastal bathymetry is provided for a few locations (see blue circles in Fig. 3 and axis from the left side of the panels for the depth values), and was interpolated by polynomial functions, see the blue curves.

NHESSD
1, 5779–5804, 2013

3 The numerical approach for simulation of weakly nonlinear waves over variable bottom

The time series of surface elevation, measured by individual gauges, contain very limited information, presenting momentary pictures of passing waves; the wave dynamics remains unrecorded. With the purpose of reconstructing the wave evolution in the vicinity of the point of measurement, in the present paper we employ weakly nonlinear equations for shoaling waves, which describe the wave transformation assuming waves propagating in one direction (shoreward). To this end we consider the nonlinear Schrodinger equation (NLS) for the case of wave evolution in space over uneven depth, which is taken into account through the depth-dependent coefficients and a shoaling term (Djordjevic and Redekopp, 1978; Zeng and Trulsen, 2012)

$$i\frac{\mathrm{d}B}{\mathrm{d}x} = -i\mu\frac{\mathrm{d}(kh)}{\mathrm{d}x}B - \frac{i}{c_\mathrm{g}}\frac{\mathrm{d}B}{\mathrm{d}t} + \lambda\frac{\mathrm{d}^2B}{\mathrm{d}t^2} + \nu|B|^2B, \tag{3}$$

$$\mu = \frac{(1-\sigma^2)(1-kh\sigma)}{\sigma + kh(1-\sigma^2)}, \qquad \lambda = \frac{1}{2c_\mathrm{g}\omega_0}\left[1 - \frac{gh}{c_\mathrm{g}^2}(1-kh\sigma)(1-\sigma^2)\right],$$

$$\nu = \frac{\omega_0 k^2}{16\sigma^2 c_\mathrm{g}}\left[9 - 10\sigma^2 + 9\sigma^4 - \frac{2\sigma^2 c_\mathrm{g}^2}{\left(gh - c_\mathrm{g}^2\right)}\left(4\frac{c_\mathrm{p}^2}{c_\mathrm{g}^2} + 4\frac{c_\mathrm{p}^2}{c_\mathrm{g}^2}(1-\sigma^2) + \frac{gh}{c_\mathrm{g}^2}(1-\sigma^2)^2\right)\right],$$

$$\sigma = \tanh(kh), \qquad c_\mathrm{p} = \frac{\omega_0}{k}, \qquad c_\mathrm{g} = \left.\frac{\partial\omega}{\partial k}\right|_{\omega=\omega_0} = \frac{1}{\sqrt{4\omega_0}}\left(g\sigma + \frac{ghk}{ch^2(kh)}\right).$$

Here $B(x,t)$ is complex amplitude of the envelope, x is the horizontal coordinate directed onshore ($x = 0$ corresponds to the shoreline and the measuring buoy is situated at $x = x_0$), t denotes the time, g is the gravity acceleration, c_p and c_g are the local phase and group velocities respectively. When h is constant, Eq. (3) tends to the classic NLS equation for waves in a constant-depth basin.

NHESSD
1, 5779–5804, 2013

It is essential that while waves propagate over variable depth, the carrier frequency, ω_0, remains constant, whereas the wavenumber, k, varies in accordance with the dispersion relation Eq. (2), hence it is a function of x, $k = k(h(x))$. As a result, the dimensionless water depth, kh is a different function of x than $h(x)$, which is plotted in Fig. 3 by a solid red line with corresponding values given at the right side of the panels. In the considered here cases the local dimensionless depth corresponds to the intermediate or relatively deep water at x_0, and corresponds to the truly deep water at the farthest position offshore. The topography at the Hsinchu station is shallower.

Note that when ω_0 persists, the group velocity c_g depends on the coordinate through the product $k(x)h(x)$, see expression for c_g in Eq. (3). Therefore coefficient μ may be written in the form

$$\mu = \frac{1}{2c_g}\frac{\mathrm{d}c_g}{\mathrm{d}(kh)}\bigg|_{\omega=\omega_0}, \tag{4}$$

and then the shoaling term (the first summand in the right-hand-side of Eq. 3) may be transformed to $-i/(2c_g)\mathrm{d}c_g/\mathrm{d}x$, hence it expresses the conservation of wave energy flux, $c_g|B|^2$, as could be expected from the linear theory.

The numerical code of the NLS Eq. (3) is implemented in the way similar to Lo and Mei (1985), Slunyaev et al. (2005), Slunyaev (2006) and Shemer et al. (2010): the split-step-Fourier method is used, and the integration in space is performed for the periodic in time domain with the help of the Runge–Kutta fourth-order method. By virtue of the integration in space the forward wave evolution is simulated; the backward evolution is obtained when the negative step of integration in space is taken.

The measured time series are used as the starting condition for simulations. The condition at x_0, complex function $B(x_0)$, is sought with the help of iterative procedure assuming the in-situ surface elevation time series, $\eta(t)$, be described by the deep-water Dysthe theory for weakly nonlinear weakly modulated wavetrains, when the second and third-order wave corrections, and also the long-scale induced wave flow are taken into account (see details of the approach in Trulsen, 2006; Slunyaev, 2005;

NHESSD
1, 5779–5804, 2013

Slunyaev et al., 2013b). Just the same, the bound wave harmonics are computed for given $B(t)$ to produce the surface elevation function $\eta(t)$ at different x. Strictly speaking, for shallow water ($kh \sim < 2$) this approach is not legitimate, then the reconstruction formulas contain cumbersome coefficients and are still challenging.

4 Reconstruction of rogue waves by means of the variable-coefficient NLS equation

The measured time series are simulated within the framework of the variable-coefficient NLS, as described above, and hence the wave evolution in the direction onshore (increasing x) and offshore is reconstructed. When waves approach the shoreline, their energy grows and at some place the wave steepness becomes unrealistically large. The wave breaking is not described by the weakly nonlinear model, and waves can grow infinitively as $h \to 0$. We stop simulations shoreward at the location of the shallowest available bathymetry data (the leftmost circles in Fig. 3); the closest to the coast location is about 130 m (for the Eluanbi buoy). In the seawards direction the simulation recovers the wave evolution backward for a few kilometers, see Fig. 3. The simulations and results of analysis of the obtained data are discussed in this section; conclusions are drawn in the subsequent Discussions.

The simulated data was stored each 2 m of the wave run, hence the output data are wave field domains of the size 512 s by from 3.5 to 6 km. The rogue wave evolution is restored by virtue of the approach, and is analyzed afterwards. This data may be used for an extensive study of the rogue wave evolution and appearance, and of mutual properties of the elevation and kinematic fields, as suggested in Sergeeva and Slunyaev (2013). Since in the course of evolution wave energy varies due to the shoaling effect, the significant wave height is calculated accordingly for the time series at particular locations, thus $H_s = H_s(x)$. In the present paper the significant wave height is estimated in the quasi-Gaussian approximation with the help of the standard deviation, $H_s = 4\eta_{rms}$ (see for details Massel, 1996, and Kharif et al., 2009).

NHESSD
1, 5779–5804, 2013

The measured rogue wave disappears apart from x_0, when its height falls below the level $2H_s(x)$. However, it may exceed this threshold shortly after, and thus it is naturally to consider the case of resuming extremely large waves as one continuous rogue wave event. The life times of such extreme events, when the condition Eq. (1) may be violated for some short periods of time (less than a coupe of wave periods), were shown to reach up to 10 min in deep-sea simulations of unidirectional Euler equations by Sergeeva and Slunyaev (2013).

Such "intermittent" rogue events are observed in the present simulations as well; an example is provided in Fig. 4 for the record from the Hsinchu buoy; time series at different locations are shown. The wave, which amplitude exceeds the significant wave height twice or more, is marked with a bold red curve. The rogue wave occurs a little bit prior the buoy location ($x_0 = -2440$ m) and propagates for about 550 m during about 60 s, from time to time exceeding the threshold $2H_s$ prescribed by the rogue wave definition Eq. (1). Quite naturally, the rogue wave shape in the simulated wave profiles changes in the course of evolution. Pictures, similar to Fig. 4, are obtained for other recorded time series. In all the simulations no cases when subsequent waves in the time series exceed the value of $2H_s$ were observed (i.e., no rogue groups). On the other hand, time series in Fig. 4 demonstrate that the rogue waves often belong to intense wave groups.

The top-views on the (x, t) fields of the surface elevation are given in Fig. 5; the elevation magnitude is shown with the colour gradation. Waves which satisfy the criterion Eq. (1) are marked with blue circles. Momentary, long-living and intermittent rogue waves may be observed in the figure; the latter are collated by red boxes. Note the periodic boundary condition for the time axis; thus when a wave reaches the right boarder of the shown domain, it continues from the left side. It is readily seen that most of the long-living rogue events occur on the background of intense trains which do not exhibit a clear dispersion of energy; this confirms observations in Sergeeva and Slunyaev (2013) for the deep-sea conditions.

NHESSD
1, 5779–5804, 2013

Eight rogue events were found in the simulations according to the condition Eq. (1), see Fig. 5. Four of them correspond to the registered rogue waves, and the others occur at distant from x_0 locations. It is important to note that all the new rogue events occur seaward, i.e., at deeper conditions; no rogue waves in the shallower areas have been found. The rogue event lifetimes and corresponding distances passed are given in Fig. 6 as functions of the abnormality index, AI = H/H_s. There are long-living extreme events which last up to 100 s and travel 600 m, and also fleeting events. Generally, rogue waves with large AI live longer.

Due to the frequent data storing, each rogue event in our numerical simulations contains up to 300 time series enclosing rogue waves. We estimate the most probable appearance of the rogue wave by considering these time series in statistical sense. Four kinds of rogue waves are distinguished: rear positive waves (RPW), rear negative waves (RNW), front positive waves (FPW), front negative waves (FNW). This classification was introduced in Sergeeva and Slunyaev (2013) and reflects the wave symmetry properties with respect to the extreme wave slope (the rogue wave crest and rogue wave through confine this slope from two sides). Thus, the front positive wave (FPW) is the wave, when the extreme slope of the height H_{fr} is the front slope, and the crest amplitude exceeds the trough amplitude. The rear negative wave (RNW) has the extreme slope at the rear side, and the trough is deeper than the height of the crest.

The diagram in Fig. 7 represents the distribution of rogue waves between these 4 types of waves for each of the eight rogue events. The figures above the columns indicate the number of time series (and, correspondingly, rogue wave shapes), used in the averaging procedure; one may see that the numbers are not always sufficiently large to provide a statistically sensible result. The major part of rogue waves is waves with high crests and shallow troughs; waves with deeper troughs are observed as well (similar to shown in Fig. 1a), though they are less numerous. The proportions of waves, when the extreme slope is at the front or the rear side of waves, are about the same.

NHESSD
1, 5779–5804, 2013

5 Discussion

The rogue wave evolution is reconstructed on the basis of in-situ instrumental records of the surface elevation in the manner similar to Trulsen (2001), Slunyaev et al. (2005, 2013b), Slunyaev (2006). To this end the asymptotic equations for surface water waves, which describe the evolution in space, are solved numerically. Waves are assumed to be unidirectional, weakly modulated and weakly nonlinear. In Slunyaev et al. (2013b) the approach was shown able to serve even in cases of fairly steep modulated waves. In contrast to the papers mentioned above, the field condition in the present situation corresponds to essentially variable bottom profile, when waves run onshore; hence the modification of the evolution equation, which takes into account the sea shoaling, is used.

In the recent numerical and partly laboratory studies wave nonlinearity has been shown able to increase significantly the probability of rogue waves both in shallow (Pelinovsky and Sergeeva, 2006) and deep water conditions (Onorato et al., 2001, 2002; Janssen, 2003; Shemer and Sergeeva, 2009, and many subsequent publications). Hence, the nonlinear wave interactions in homogeneous conditions may lead to a higher risk of rogue wave occurrence.

When waves travel from deep to shallow areas, the energy gets amplified due to the change of propagation velocity. This is a classical quasi-linear effect; it is captured by the NLS Eq. (3). Figure 8 shows the dependence of wave energy in our simulation when waves are approaching the coast, through the quantity $8\eta_{\mathrm{rms}}$ (thick black line) for the condition of the Hsinchu station. The energy grows further when the depth becomes even shallower; at some point the step of numerical integration becomes too coarse and the simulation becomes inaccurate.

At first glance, it is reasonable to expect that this intensification effect would result in occurrence of a greater number of rogue waves shoreward due to the increase of wave amplitude. Numerical and laboratory simulations by Sergeeva et al. (2011), Zeng and Trusen (2012), Trulsen et al. (2012) of irregular nonlinear waves, undergoing

NHESSD
1, 5779–5804, 2013

bottom variations in the form of a smooth step, draw a more complicated picture, still to be comprehended in full. The bottom variability can lead to significant changes of statistical properties of the wave field; the relatively fast change of the waveguide conditions can make the wave dynamics extreme. In particular, the statistical moments may increase at the shallower region and then the likelihood of extreme wave heights increases as well. In some situations significant increase of rogue wave occurrence was observed indeed, though in other cases no significant changes were found. Zeng and Trulsen (2012) considered a "deeper" regime ($kh > 1.2$) of wave evolution compared to numerical simulations by Sergeeva et al. (2011) ($kh < 0.4$) and exposed the reduced kurtosis and skewness for the shallower region of transformation. The laboratory experiments on the wave propagation from deeper to shallower zone set by Trulsen et al. (2012) embrace the "transitional" zone when the waves travel from intermediate depth to the shallow water with kh down to 0.54. An increase of large wave likelihood and kurtosis was observed for the smallest dimensionless depth in the experiment, $kh = 0.54$. The shallow water conditions of kh equal to 0.7 and 0.99 demonstrated the decrease of these statistical parameters. Let us note an interesting peculiarity of gravity waves: the wave group velocity possesses the maxima at $kh \approx 1.2$ and gets somewhat smaller over deeper seas and much smaller in coastal waters. Thus the linear theory predicts that waves propagating onshore from the deep water should somewhat diminish at $kh \approx 1.2$.

When waves travel from deep to shallow water, the problem is controlled by the following dimensionless parameters: initial and final local depths, the Ursell parameter and the Benjamin–Feir index (BFI). The Benjamin–Feir index may be written in form taking into account the depth finiteness,

$$\mathrm{BFI} = \sqrt{2}\frac{k\eta_{\mathrm{rms}}}{\Delta\omega/\omega_0}\frac{\nu}{\lambda\omega_0^2 k^2} \tag{5}$$

here ν and λ are coefficients specified in Eq. (3), the right multiplier in Eq. (5) tends to one in the limit of infinite depth. The BFI characterizes the importance of nonlinear

NHESSD
1, 5779–5804, 2013

effects due to 4-wave resonances with respect to the wave dispersion. Uniform waves become modulationally unstable when BFI > 1; BFI becomes less than zero when kh decays lower than 1.363 due to the change of coefficient ν, see details in Slunyaev et al. (2002) or textbook (Johnson, 1997).

We emphasize that when the sea is deep ($kh \gg 1$), envelope solitons are exact solutions of the NLS equation with constant coefficients. These solutions are wave groups which in the theory may propagate eternally, and rather long in realistic conditions (see Slunyaev et al., 2013a, and references therein). The long-living intense wave groups in irregular unidirectional waves over deep water are believed to be related to the NLS solitons, see results in Slunyaev and Sergeeva (2011). The long-living wave groups clearly observed in Fig. 6 resemble very much soliton-like groups, which are transforming due to the variable conditions. At the same time, the BFI calculated at the conditions of instrumental measurements are quite small, see Table 1; the Hsinchu station is located at condition $kh < 1.363$, and thus the index has negative value. When the sea shallows, the nonlinear coefficient in the NLS equation gets smaller so that BFI decays as well, what reduces the self-focusing effect. As a result, solitary groups of given amplitude consist of a greater number of waves, see Slunyaev et al. (2002), Didenkulova et al. (2013); when $kh < 1.363$ solitary groups are not solutions for the NLS equation. It is known that envelope solitons disperse when the depth becomes less than $kh < 1.363$ (Grimshaw and Annenkov, 2011); therefore the role of solitary groups is expected to diminish as $kh \sim< 2$, when the coefficients of the NLS equation differ significantly from the deep-water values. The values of BFI observed in all the reported simulations remain less than 0.17.

As water becomes shallow, three-wave resonances start to play the major role; the importance of the shallow-water nonlinearity is controlled by the Ursell parameter, which may be written in form

$$Ur = \frac{4\pi^2 gH}{\omega^2 h^2}. \quad (6)$$

NHESSD
1, 5779–5804, 2013

The Stokes wave theory requires $Ur < 10$, see (Holthuijsen, 2007). When Ur is too large, the NLS theory for modulated waves becomes inapplicable (when $Ur > 26$, according to Holthuijsen, 2007). This parameter is calculated for the measured time series taking in Eq. (6) $H = 4\eta_{\mathrm{rms}}$ and $\omega = \omega_{\mathrm{p}}$; indeed, the values of Ur at the measurement locations are sufficiently small to employ the NLS theory, see Table 1. In the shallow water limit $kh \ll 1$ the conservation of energy flux results in Green's law in form $H(x)/H(x_0) = (h(x_0)/h(x))^{1/4}$, and the Ursell number grows as the sea becomes shallower. In the numerical simulations the Ursell numbers remain very small ($Ur < 2$) in cases of Hualien, Elaunbi and Longdong buoys; in contrast, the waves from Hsinchu buoy attain very large value $Ur \approx 38$ at the shallowest available bathymetry location $kh \approx 0.66$.

All the four numerical simulations reported by us exhibit the situation when coastal rogue waves occur more frequent at deeper locations, see Fig. 5. Figure 8 reports on the dependences of maximum wave heights in the simulations of the variable NLS equation (the thin black curve) vs. dimensionless depth, kh. The bold line shows the dependence of $8\eta_{\mathrm{rms}}$, which characterizes the evolution of the mean wave amplitude. The sea depth at the registration point is rather shallow in the case of Hsinchu buoy ($k_{\mathrm{p}}h = 1.34$). Despite the confident growth of the average wave intensity close to the coast, the wave heights do not overpass the limit $8\eta_{\mathrm{rms}}$.

Due to the large number of controlling parameters, the conclusion which is drawn from the present simulations cannot be considered general: other combinations of wave intensity and bathymetry peculiarities might result in opposite effect, when the rogue wave probability increases as waves propagate shoreward.

Acknowledgements. This study is supported by the Russian-Taiwanese grant (RFBR 11-05-9202 and NSC 100-2923-M-019-001). For Russian authors support by RFBR grants (12-05-33087, 11-02-00483, 11-05-00216, and 13-05-97037) is acknowledgement. A. Sergeeva and E. Pelinovsky would like to acknowledge support from the Volkswagen Foundation. A. Sergeeva thanks the support from grant MK-5222.2013.5.

NHESSD
1, 5779–5804, 2013

References

Chang, F. S.: Analysis of oceanic rogue waves from in-situ measurements, M.Sc. thesis, National Taiwan Ocean University, Keelung, Taiwan, 2012.

Didenkulova, I. I., Nikolkina, I. F., and Pelinovsky, E. N.: Rogue waves in the basin of intermediate depth and the possibility of their formation due to the modulational instability, JETP Lett., 97, 194–198, doi:10.1134/S0021364013040024, 2013.

Divinsky, B. V., Levin, B. V., Lopatukhin, L. I., Pelinovsky, E. N., and Slyunyaev, A. V.: A freak wave in the Black sea: observations and simulation, Dokl. Earth. Sci. A, 395, 438–443, 2004.

Djordjevic, V. D. and Redekopp, L. G.: On the development of packets of surface gravity waves moving over an uneven bottom, J. Appl. Math. Phys., 29, 950–962, 1978.

Doong, D. J., Chen, S. H., Kao, C. C., and Lee, B. C.: Data quality check procedures of an Operational Coastal Ocean Monitoring Network, Ocean Eng., 34, 234–246, 2007.

Doong, D. J., Tseng, L. H., and Kao, C. C.: A study on the oceanic freak waves observed in the field, in: Proceedings of the 8th International Conference on Coastal and Port Engineering in Developing Countries (PIANC-COPEDEC VIII), 20–24 February 2012, IIT Madras, Chennai, India, 301–308, 2012.

Dysthe, K., Krogstad, H. E., and Muller, P.: Oceanic rogue waves, Annu. Rev. Fluid. Mech., 40, 287–310, 2008.

Grimshaw, R. H. J. and Annenkov, S. Y.: Water wave packets over variable depth, Stud. Appl. Math., 126, 409–427, 2011.

Holthuijsen, L. H.: Waves in Oceanic and Coastal Waters, Cambridge Univ. Press, New York, 2007.

Janssen, P. A. E. M.: Nonlinear four wave interactions and freak waves, J. Phys. Oceanogr., 33, 863–884, 2003.

Johnson, R. S.: A Modern Introduction to the Mathematical Theory of Water Waves, Cambridge Univ. Press, Cambridge, 1997.

Kharif, C. and Pelinovsky, E.: Physical mechanisms of the rogue wave phenomenon, Eur. J. Mech. B, 22, 603–634, 2003.

Kharif, C., Pelinovsky, E., and Slunyaev, A.: Rogue Waves in the Ocean, Springer, Berlin, 2009.

Lee, B. C., Kao, C. C., and Doong, D. J.: An analysis of the characteristics of freak waves using the wavelet transform, Terr. Atmos. Ocean. Sci., 22, 359–370, 2011.

NHESSD
1, 5779–5804, 2013

Lo, E. and Mei, C. C.: A numerical study of water-wave modulation based on a higher-order nonlinear Schrödinger equation, J. Fluid Mech., 150, 395–416, 1985.
Massel, S. R.: Ocean Surface Waves: their Physics and Prediction, World Scientific, Singapore, 1996.
Onorato, M., Osborne, A. R., Serio, M., and Bertone, S.: Freak waves in random oceanic sea states, Phys. Rev. Lett., 86, 5831–5834, 2001.
Onorato, M., Osborne, A. R., and Serio, M.: Extreme wave events in directional, random oceanic sea states, Phys. Fluids, 14, 25–28, 2002.
Pelinovsky, E. and Sergeeva, A.: Numerical modeling of the KdV random wave field, Eur. J. Mech. B, 25, 425–434, 2006.
Sergeeva, A. and Slunyaev, A.: Rogue waves, rogue events and extreme wave kinematics in spatio-temporal fields of simulated sea states, Nat. Hazards Earth Syst. Sci., 13, 1759–1771, doi:10.5194/nhess-13-1759-2013, 2013.
Sergeeva, A., Pelinovsky, E., and Talipova, T.: Nonlinear random wave field in shallow water: variable Korteweg–de Vries framework, Nat. Hazards Earth Syst. Sci., 11, 323–330, doi:10.5194/nhess-11-323-2011, 2011.
Shemer, L. and Sergeeva, A.: An experimental study of spatial evolution of statistical parameters of unidirectional narrow-banded random wave field, J. Geophys. Res., 114, C01015, doi:10.1029/2008JC005077, 2009.
Shemer, L., Sergeeva, A., and Slunyaev, A.: Applicability of envelope model equations for simulation of narrow-spectrum unidirectional random field evolution: experimental validation, Phys. Fluids, 22, 016601, 1–9, doi:10.1063/1.3290240, 2010.
Slunyaev, A. V.: A high-order nonlinear envelope equation for gravity waves in finite-depth water, J. Exp. Theor. Phys., 101, 926–941, 2005.
Slunyaev, A.: Nonlinear analysis and simulations of measured freak wave time series, Eur. J. Mech. B, 25, 621–635, 2006.
Slunyaev, A. V. and Sergeeva, A. V.: Stochastic simulation of unidirectional intense waves in deep water applied to rogue waves, JETP Lett., 94, 779–786, doi:10.1134/S0021364011220103, 2011.
Slunyaev, A., Kharif, C., Pelinovsky, E., and Talipova, T.: Nonlinear wave focusing on water of finite depth, Physica D, 173, 77–96, 2002.
Slunyaev, A., Pelinovsky, E., and Guedes Soares, C.: Modeling freak waves from the North Sea, Appl. Ocean Res., 27, 12–22, 2005.

NHESSD
1, 5779–5804, 2013

Slunyaev, A., Didenkulova, I., and Pelinovsky, E.: Rogue Waters, Contemp. Phys., 52, 571–590, 2011.
Slunyaev, A., Clauss, G. F., Klein, M., and Onorato, G. F.: Simulations and experiments of short intense envelope solitons of surface water waves, Phys. Fluids, 25, 067105, 1–17, doi:10.1063/1.4811493, 2013a.
Slunyaev, A., Pelinovsky, E., and Guedes Soares, C.: Reconstruction of extreme events through numerical simulations, J. Offshore Mech. Arct., in press, doi:10.1115/1.4025545, 2013b.
Trulsen, K.: Simulating the spatial evolution of a measured time series of a freak wave, in: Proceedings of the workshop "Rogue Waves 2000", edited by: Olagnon, M. and Athanassoulis, G. A., Brest, France, 29–30 November 2000, 265–274, 2001 .
Trulsen, K.: Weakly nonlinear and stochastic properties of ocean wave fields: application to an extreme wave event, in: Waves in Geophysical Fluids: Tsunamis, Rogue Waves, Internal Waves and Internal Tides, edited by: Grue, J. and Trulsen, K., CISM Courses and Lectures No. 489, 49–106, Springer, New York, 2006.
Trulsen, K., Zeng, H., and Gramstad, O.: Laboratory evidence of freak waves provoked by non-uniform bathymetry, Phys. Fluids, 24, 097101, doi:10.1063/1.4748346, 2012.
Zeng, H. and Trulsen, K.: Evolution of skewness and kurtosis of weakly nonlinear unidirectional waves over a sloping bottom, Nat. Hazards Earth Syst. Sci., 12, 631–638, doi:10.5194/nhess-12-631-2012, 2012.

NHESSD
1, 5779–5804, 2013

Table 1. Main parameters of the in-situ records.

	h [m]	$-x_0$ [km]	$k_p h$	T_p [s]	T_{fr} [s]	λ_{fr} [m]	H_{fr} [m]	H_{fr}^{cr} [m]	H_s [m]	Ur	BFI
1. Hsinchu	26.5	2.5	1.34	9.5	8.8	122	6.2	2.7	3.0	1.26	−0.022
2. Hualien	30	1	1.9	8.1	7.3	99	3.2	1.7	1.4	0.24	0.032
3. Eluanbi	40	2	2.3	8.5	7.3	111	3.4	1.5	1.4	0.14	0.050
4. Longdong	42	1	4.0	6.5	6.3	66	2.8	1.6	1.3	0.04	0.136

NHESSD
1, 5779–5804, 2013

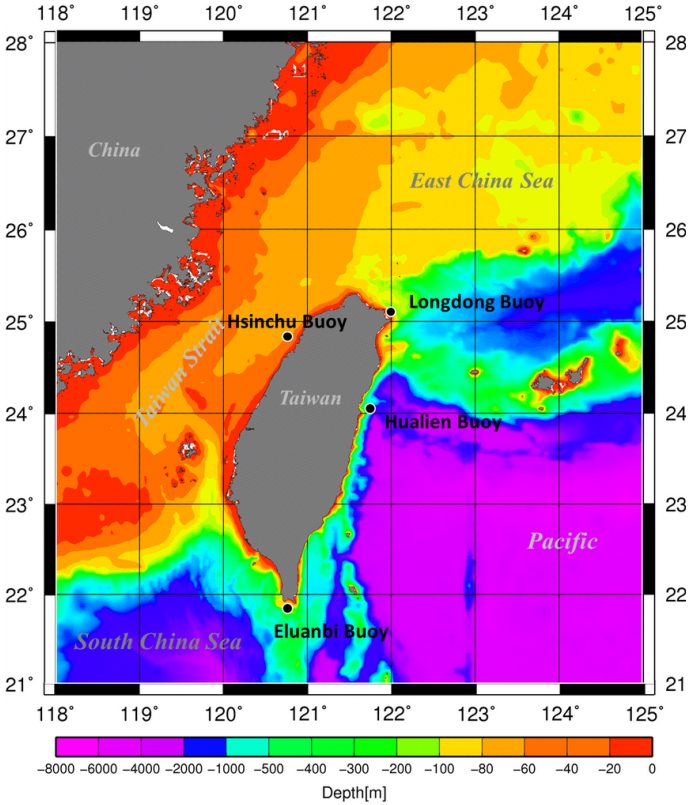

Fig. 1. Locations of the buoys used in this study.

NHESSD
1, 5779–5804, 2013

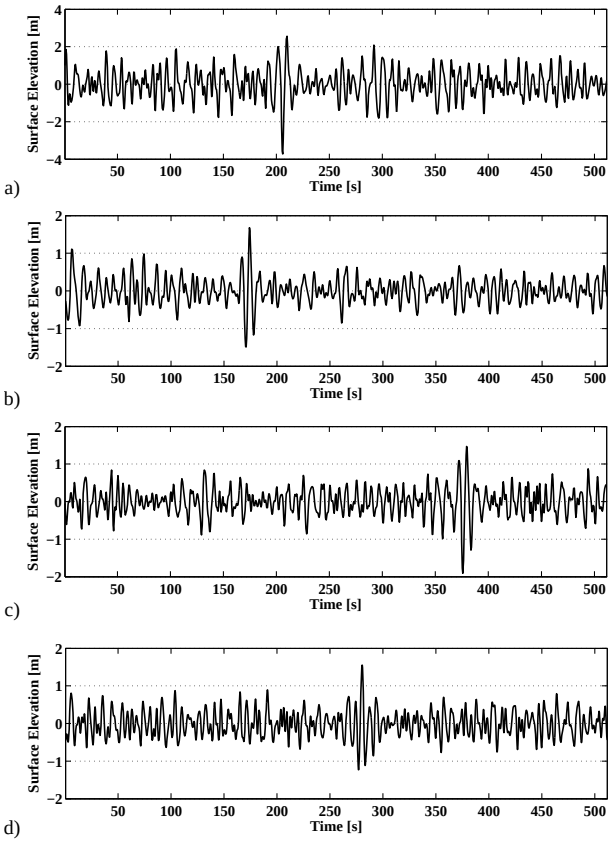

Fig. 2. Instrumental time series containing rogue waves, retrieved at locations: **(a)** Hsinchu, **(b)** Hualien, **(c)** Elaunbi, **(d)** Longdong.

NHESSD
1, 5779–5804, 2013

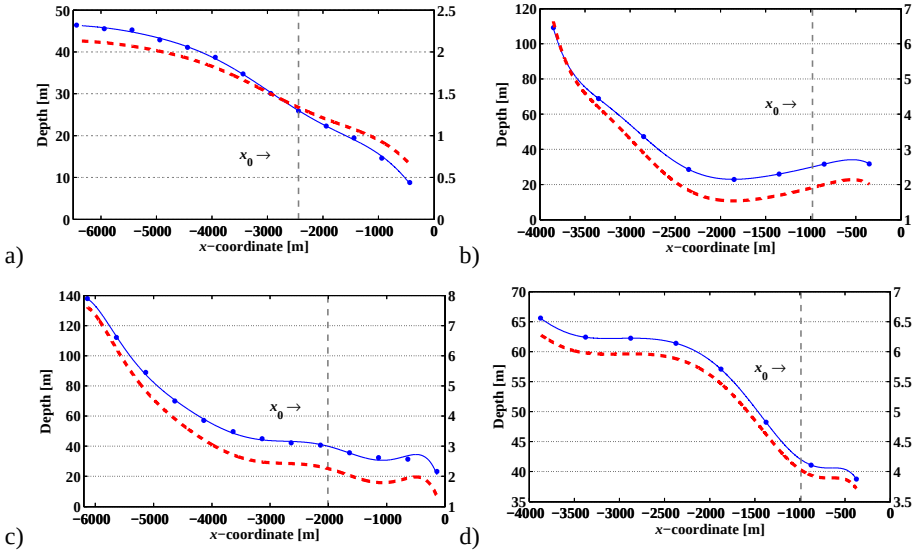

Fig. 3. The uneven bathymetry for the locations of measurements. The circles and the connecting blue lines show the depth (the left axis), while the local dimensionless water depth (kh) is shown with red curves and corresponding right-side axis. The vertical lines denote the measurement positions x_0. Locations: **(a)** Hsinchu, **(b)** Hualien, **(c)** Elaunbi, **(d)** Longdong.

NHESSD
1, 5779–5804, 2013

Numerical modeling of rogue waves in coastal waters

A. Sergeeva et al.

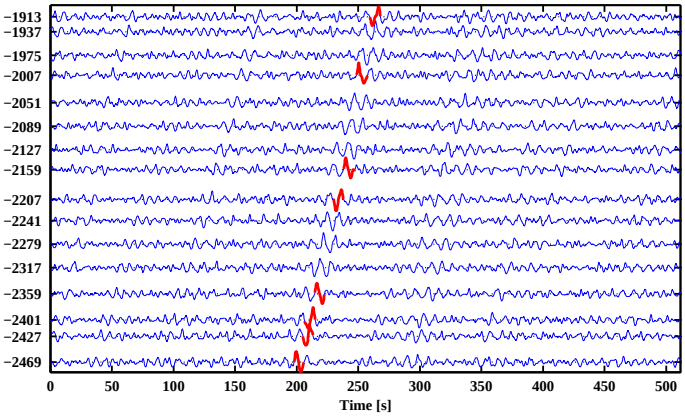

Fig. 4. The simulated rogue wave evolution, record from the Hsinchu buoy. Numbers at the left side give values of x in meters. The thick red curves show waves, which satisfy criterion Eq. (1) for local x.

NHESSD
1, 5779–5804, 2013

Numerical modeling of rogue waves in coastal waters

A. Sergeeva et al.

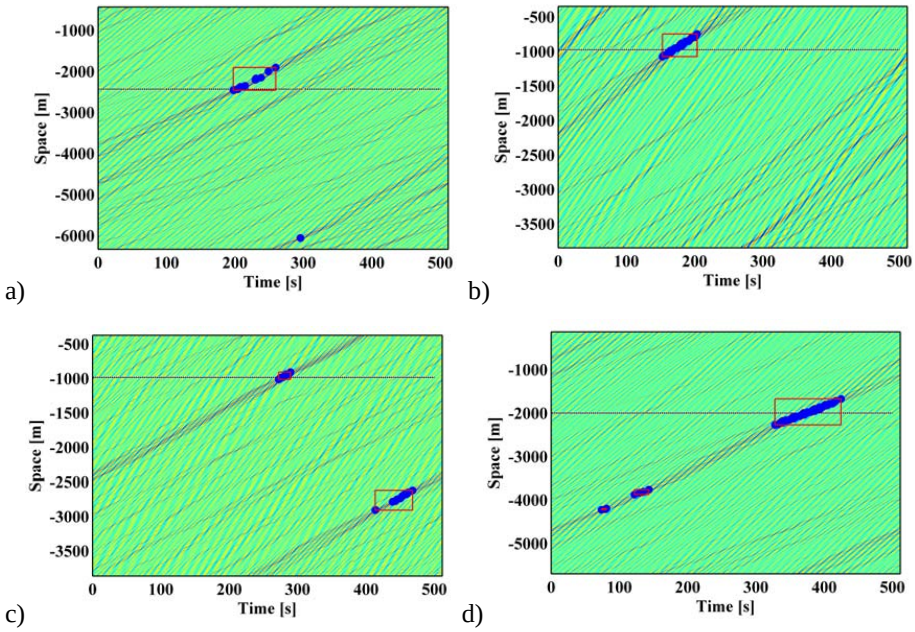

Fig. 5. The spatio-temporal fields of surface elevations with rogue waves shown by blue circles and long-term rogue events collided by red boxes. Simulations of records from the Hsinchu **(a)**, Hualien **(b)**, Longdong **(c)** and Eluanbi **(d)** buoys. Horizontal lines indicate coordinates of the in-situ measurements.

NHESSD
1, 5779–5804, 2013

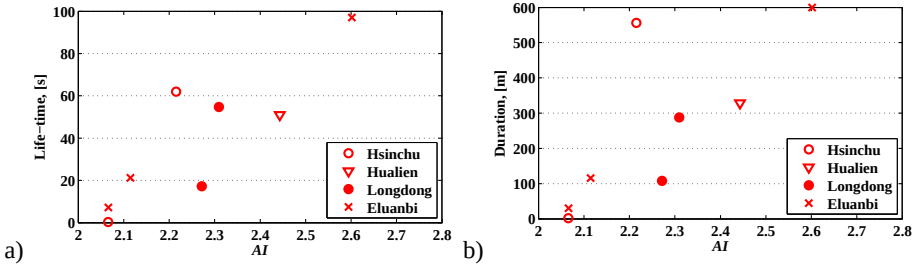

Fig. 6. Life-times **(a)** and passed distances **(b)** of rogue events in the simulated data vs. the abnormality index, AI.

NHESSD
1, 5779–5804, 2013

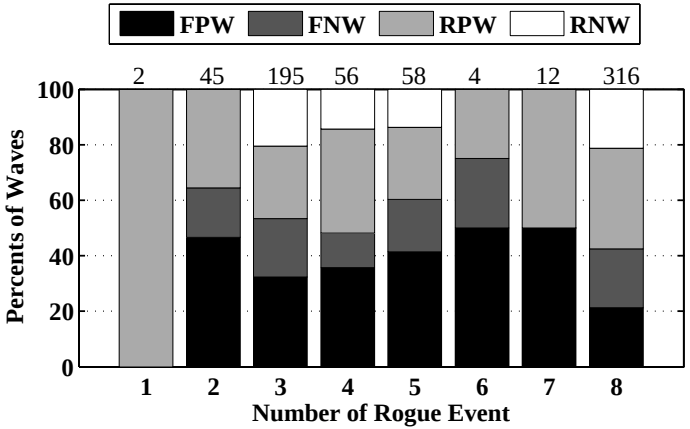

Fig. 7. Distribution of different kinds of wave appearance observed in 8 rogue events. Numbers above the columns indicate the volume of the statistical ensemble. RPW = “rear positive wave”, RNW = “rear negative wave”, FPW = “front positive wave”, FNW = “front negative wave”.

NHESSD
1, 5779–5804, 2013

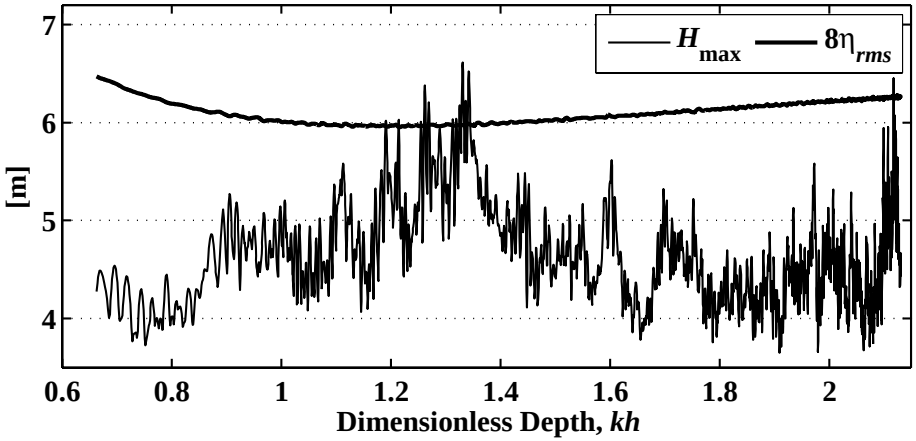

Fig. 8. Maximum wave heights vs. dimensionless sea depth observed in the numerical simulations of the NLS; the thick lines give values of $8\eta_{\text{rms}}$. Simulations of record from the Hsinchu buoy.

NHESSD
1, 5779–5804, 2013